INSTITUTE OF PLASMA PHYSICS
CZECHOSLOVAK ACADEMY OF SCIENCES

TEST OF THE QUASI-OPTICAL GRILL FOR LOWER HYBRID CURRENT DRIVE ON THE CASTOR TOKAMAK

Klíma R., Pavlo P., Preinhaelter, J. Stöckel, Žáček F.,
Jakubka K., Kletečka P., Kryška L.

IPPCZ - 337

March 1994

RESEARCH REPORT

POD VODÁRENSKOU VĚŽÍ 4, 180 69 PRAGUE 8
CZECHOSLOVAKIA

TEST OF THE QUASI-OPTICAL GRILL FOR LOWER HYBRID CURRENT DRIVE ON THE CASTOR TOKAMAK

Klíma R., Pavlo P., Preinhaelter, J. Stöckel, Žáček F.
Jakubka K., Kletečka P., Kryška L.

IPPCZ-337 March 1994

Test of the quasi-optical grill for lower hybrid current drive on the CASTOR tokamak

Klíma R., Pavlo P., Preinhaelter J., Stöckel J., Žáček F., Jakubka K., Kletečka P.,, Kryška L.
Institute of Plasma Physics, Za Slovankou 3, 182 00 Prague 8, Czech Republic

INTRODUCTION:

Slow lower hybrid waves (LHW) are used as a promising method of the non-inductive current drive and current profile control in tokamaks. However, the complexity of the launching structures available at present (phased arrays of waveguides, so called waveguide grills), represents a serious technical obstacle for their application on the next step machines. A development of simpler coupling structures could significantly enhance the attractiveness of lower hybrid current drive (LHCD) for the future thermonuclear reactor.

Being aware of this fact, the LHCD-team of JET (Joint European Torus) initiated activities to check the viability of other two, much more simple, launching systems: hyperguide [1] and diffraction system [2]. The second one, the so called quasioptical grill, will be tested on the Prague tokamak CASTOR [3]. This test should demonstrate the possibility to launch a slow LHW into a real plasma and finally to demonstrate the current drive. The submitted report describes the progress of the work and results obtained on this field during the period October 1993 - March 1994.

The structure of this Progress Report is following. The first section presents the choice of the quasi-optical grill dimensions for the CASTOR tokamak conditions. The second section gives the results of the stand measurements of the wave radiated by the antenna with the parabolic cylindrical reflector in the presence of the still non-optimized one or two rows of straight rods. The third section deals with the design of an antenna taking into account the relatively great curvature of the plasma surface in CASTOR. The ray-tracing of the launched LHW in the real CASTOR plasma is presented in section four. Finally, the last section describes probe measurements performed in the CASTOR core plasma.

1 Choice of the grill dimensions

The grill period (=the distance of the rods axes) can be determined from the Floquet's theorem. For a plane grill, this period is

$$d = \lambda/(N_{\|} + sin\alpha),$$

where λ is the wave-length of the incident wave, $N_{\|}$ is the usual index of the desired lower hybrid wave (mode m=-1 of the structure) and α is the angle of incidence. The following table gives the values of d and kd ($k = 2\pi/\lambda$ for various values of $N_{\|}$, the frequency f=9.3GHz being assumed:

$N_{\|}$	2	2.5	3	3.5	4
$d\ (cm)$	1.33	1.1	0.94	0.82	0.73
$k \cdot d$	2.6	2.15	1.84	1.6	1.42

According to our previous considerations [3] and to the ray-tracing results presented in this Report, experiments should start with $N_{\|} \simeq 3.5$.

The proper distance of the antireflection rods from the plane of the plasma facing rods is [2]

$$D_2 \simeq \lambda/2cos\alpha.$$

For the angle of incidence $\alpha = 25^o$,

$$D_2 \simeq 1.8cm.$$

Due to the finite thickness of rods, this distance must be enlarged. Consequently, we expect

$$D_2 \simeq 2.5 - 3.2cm.$$

Proper radii a_1 and a_2 of the plasma facing rods and of the antireflection rods, respectively, can be found only by computer solution and optimization of the whole task in question. Certain guides yield the results [2,4,5], where, unfortunately for our purposes, the angle of incidence 45^o and $N_{\|}$ values much lower than 3.5 are mostly used. Therefore, the following choice of the rods dimensions (for $N_{\|} = 3.5$) has no solid basis:

$2a_1 = 0.5cm$
$2a_2 =$ 1st variant: $0.5cm$
2nd variant: $0.7 - 0.75cm$.

These values have been chosen after more or less intuitive considerations in view of the fact that the values $ka_1 \simeq 0.8, ka_2 \simeq 1.2$ give good results for $kd \simeq 2.6$ [4,5].

2 Stand measurements of the wave radiated by the antenna with the parabolic cylindrical reflector

For the stand measurements of the equiphase surfaces and power pattern of the wave radiated by the antenna, shown in Fig.1, a commercial Hewlett Packard reflection and

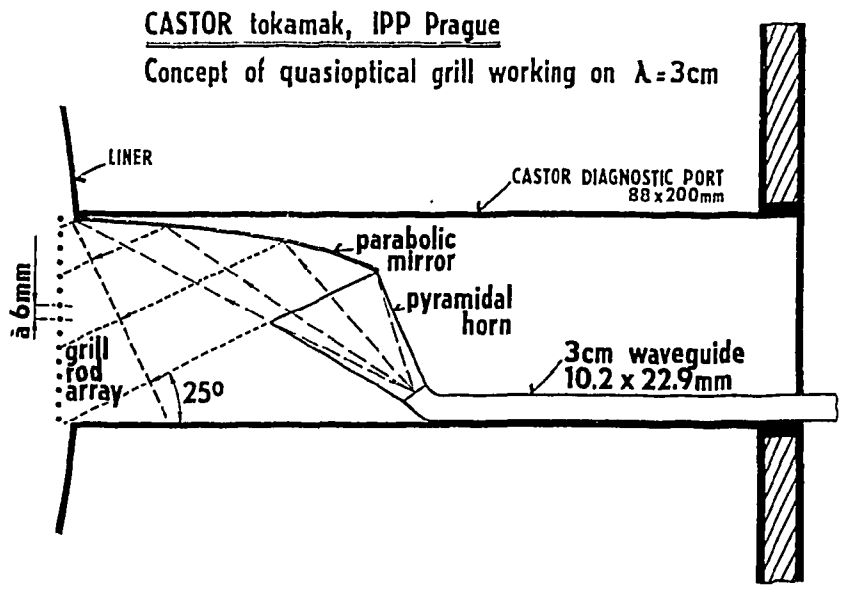

Figure 1: A schematic sketch of the launching system in the CASTOR tokamak.

transmission unit has been used. The experimental set-up of this measurements is given in Fig.2. The probing RF electrical probe has a radius 0.5mm and length 5-10mm. The probe is moved by fixing it to a plotter carriage, which position is controlled by computer during the data collection. For the mapping of the chosen region in the middle E-plane of the antenna (usually about 50x100mm, but generally different according to the interest and experimental arrangement) the matrix of 150x50 values of the wave phase and square of the electric field amplitude is registered and stored. For the data processing a standard equiplot program is applied. The 20° steps are used in the equiphase plots and $2dB$ in the equiamplitude plots mostly in all following figures (it is shown if differs).

The first measurements have concerned the antenna without the grill (i.e. without any row of metal rods) and without the box-limiter intended later for the control of the plasma profile in front of the grill, see section 5 below. The reason was to estimate in what degree the wave radiated by the suggested antenna (pyramidal horn and parabolic cylindrical reflector, see Fig.1) can be considered to be a plane one. An example of this measurements is given in Fig.3a,b. Fig.3a shows a phase and Fig.3b the amplitude of the radiated wave. It may be seen from the figure that in the region where the grill rods will be placed, the plane wave approximation is fulfilled quite reasonable. The angle of

wave propagation is found to be close to that 25° designed in Fig.1. Let us note, that in the perpendicular H-plane (where the reflector is not curved), the antenna exhibits a divergent beam with total angle of about 40°. Such angle of divergence corresponds fully to the aperture 80(x40)mm and length 50mm of the pyramidal horn.

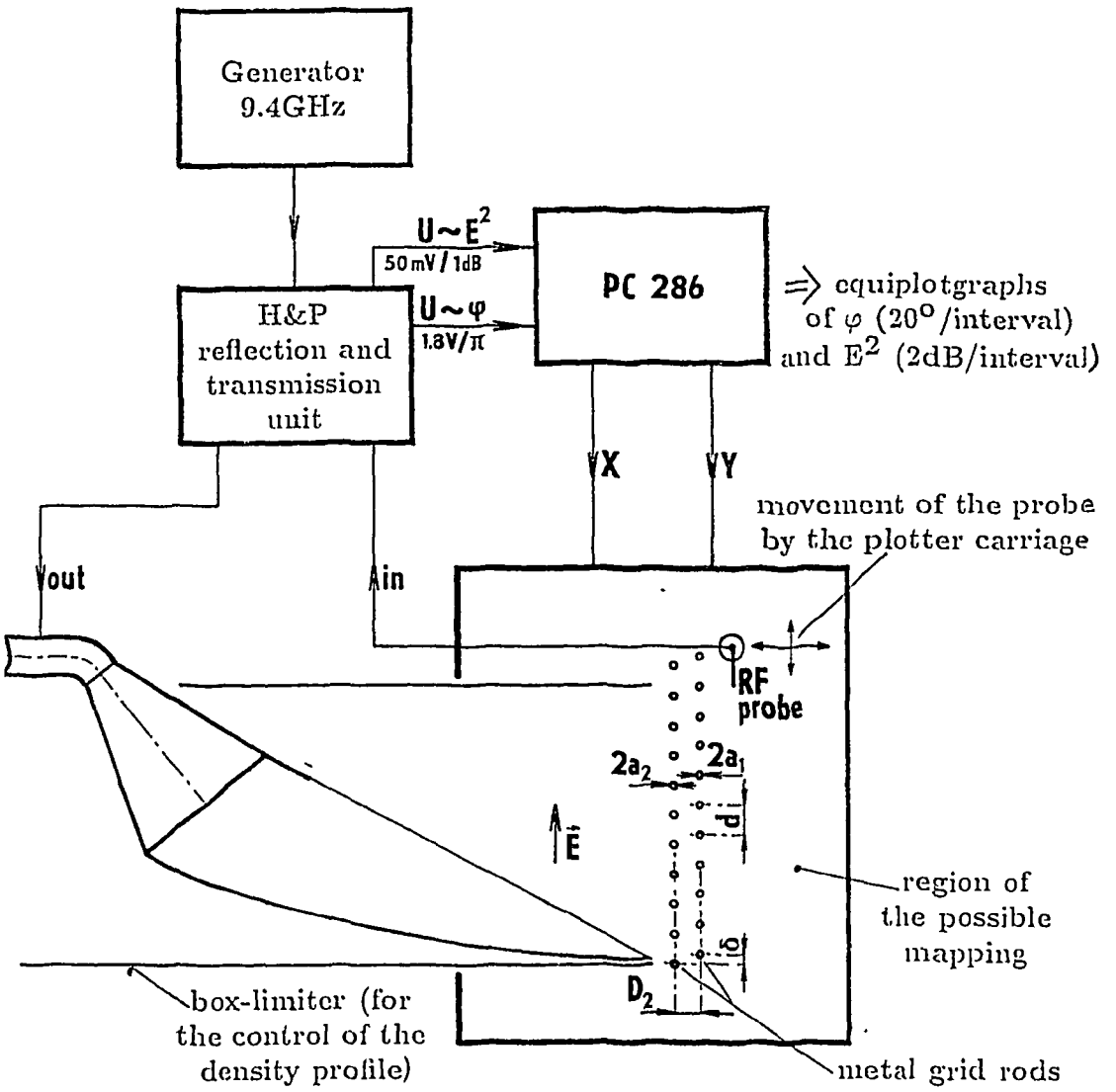

Figure 2: Experimental arrangement of the stand measurements of the wave radiated by the antenna.

As the next step, the antenna was surrounded by the box-limiter, see Fig.4. A significant distortion of the wave front is observable in this case due to the reflection on the limiter wall opposite to the reflector (see the creation of the deep node nearly $-20dB$ comparing to the amplitude in Fig.3). The attempts to cover this part of limiter by absorbing material (not vacuum compatible up to now) were not quite successful, see Fig.5, despite the fact that minimum in the node increased about $18dB$ comparing the previous

case. For this reason all the following measurements discussed below concern the case without box-limiter only.

An important question is the effect of the metal grill rods on the field pattern. Because no theoretical design is available up to now, the grill consisting of one row of 12 steel straight rods (length 10mm) with diameter $2a = 2.5mm$, placed at the distance $d = 7.5mm$, has been chosen (see section 1). The results are given in Fig.6a (phase) and Fig.7a (amplitude). The exact position of the metal rods is indicated in the figures as well. For illustrative comparison Fig.6b and Fig.7b show the situation for the case without metal rods (only internal region, in front of the reflector, is mapped in this case). It may be seen very clearly from the Figs.6 and 7 that some part of the power impinging on the grill is reflected. The relative value of this power can be determined, in principle, from both distortion of the phase surfaces (see Fig.6) and from the standing wave ratio (see Fig.7) as well. The first estimates show this power to be at the level 10-20% ($2a = 2.5mm$). The rest of the power penetrates through the grill (see Figs.6a,7a). The more detailed interpretation of the results is under preparation.

As the next step the effect of a double layer grill on the field characteristics was examined. For this purpose the second identical row of metal rods with the same diameter $2a = 2.5mm$ in a distance $D_2$was added (see Fig.2). The preliminary results of these measurements are following:

- As expected from the theory, the level of reflection depends on the distance D_2 between the two rows substantially. For $D_2 = 26mm$ hardly any reflections are observable. Let us note that similar result was obtained if the power reflected back into the horn antenna in dependence on D_2 was registered.
- Hardly any dependence of the reflection on the mutual shift δ (see Fig.2) of the two rows was observable (for $2a = 2.5mm$).

As follows from the rough estimates given in preceeding section 1, the thickness of the rods must be chosen much larger. For this reason, the measurements with another grill are now going (diameter of the rods $2a = 5mm$). After the experiments with the grill matching, an attempt to launch the slow wave into a water slab is envisaged.

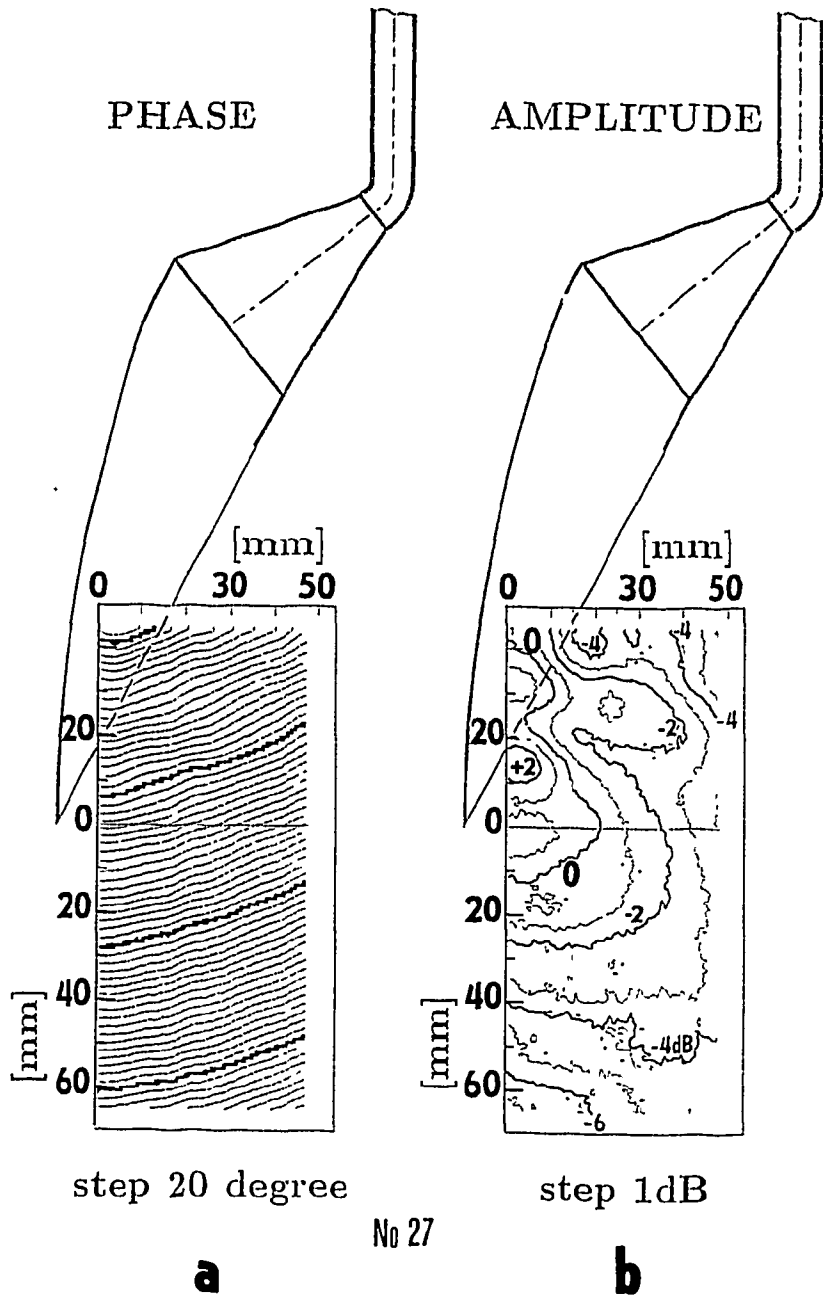

Figure 3: The map of the field radiated by the antenna consisted of pyramidal horn equipped by the parabolic cylindrical reflector; a - equiphase surfaces (360° between two more expressive curves); b - radiation pattern (strictly speaking the signal proportional to the square of the electric field amplitude).

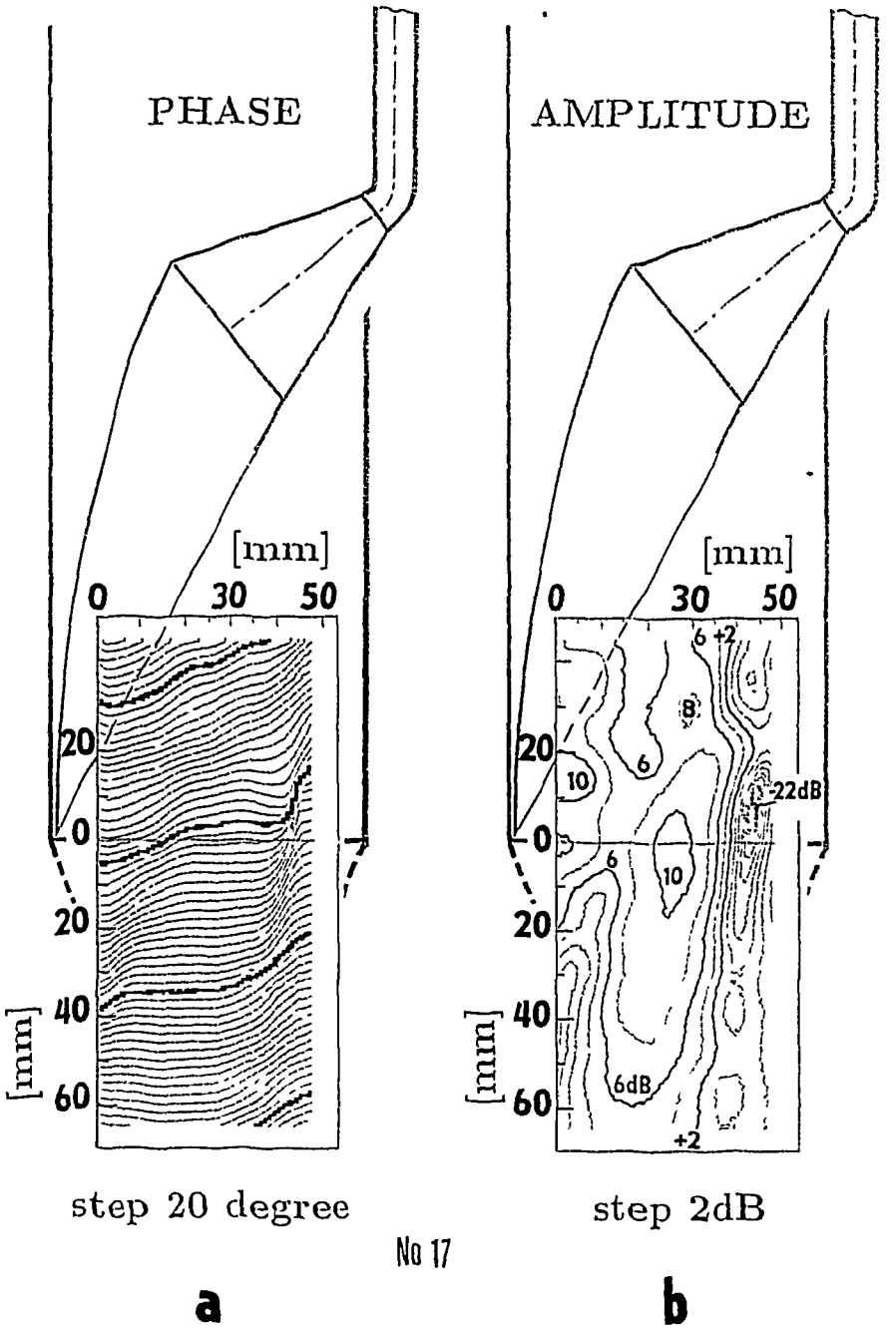

Figure 4: The map of the field radiated by the same antenna as in Fig.3, but placed in the box-limiter in this case.

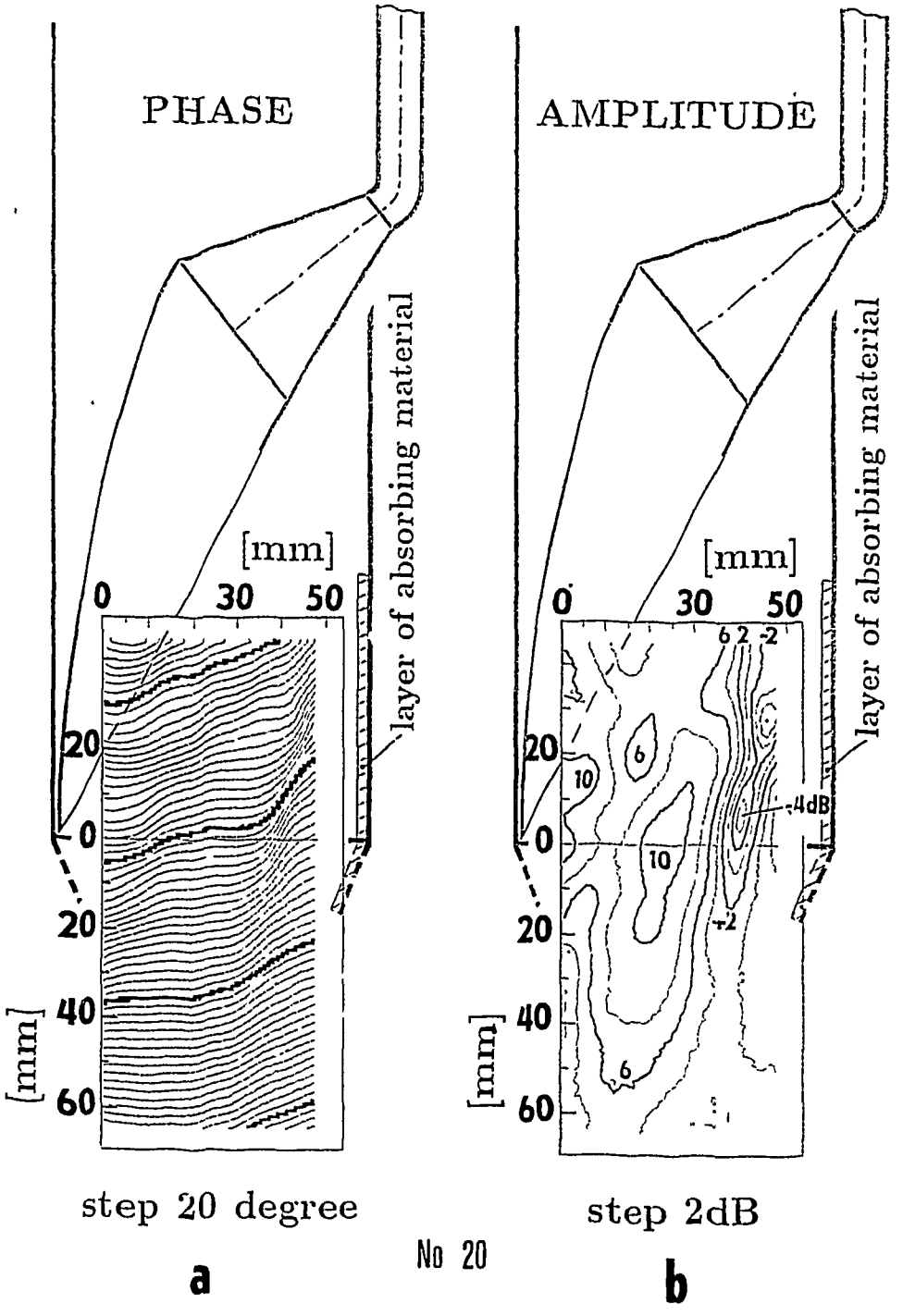

Figure 5: The same map as in Fig.4 in the case of covering of a part of the box-limiter wall (indicated in the figure) by the absorbing material (polyuretan foam soaked in a kolloidgraphit solution).

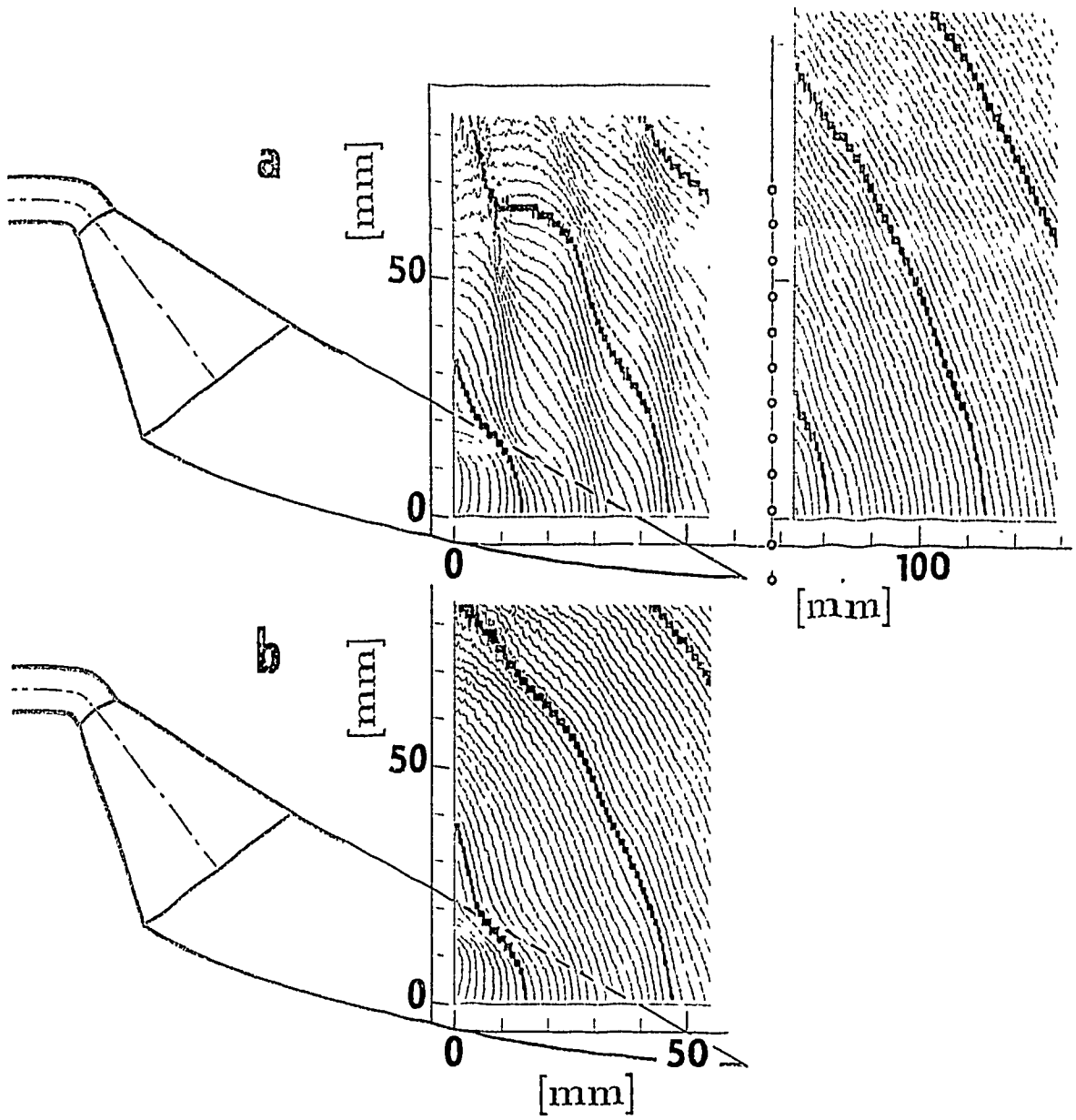

Figure 6: The equiphase surfaces of the field radiated by the antenna without box-limiter: a - in the presence of one row of metal rods (position of the row is indicated in the figure); b - without rods.

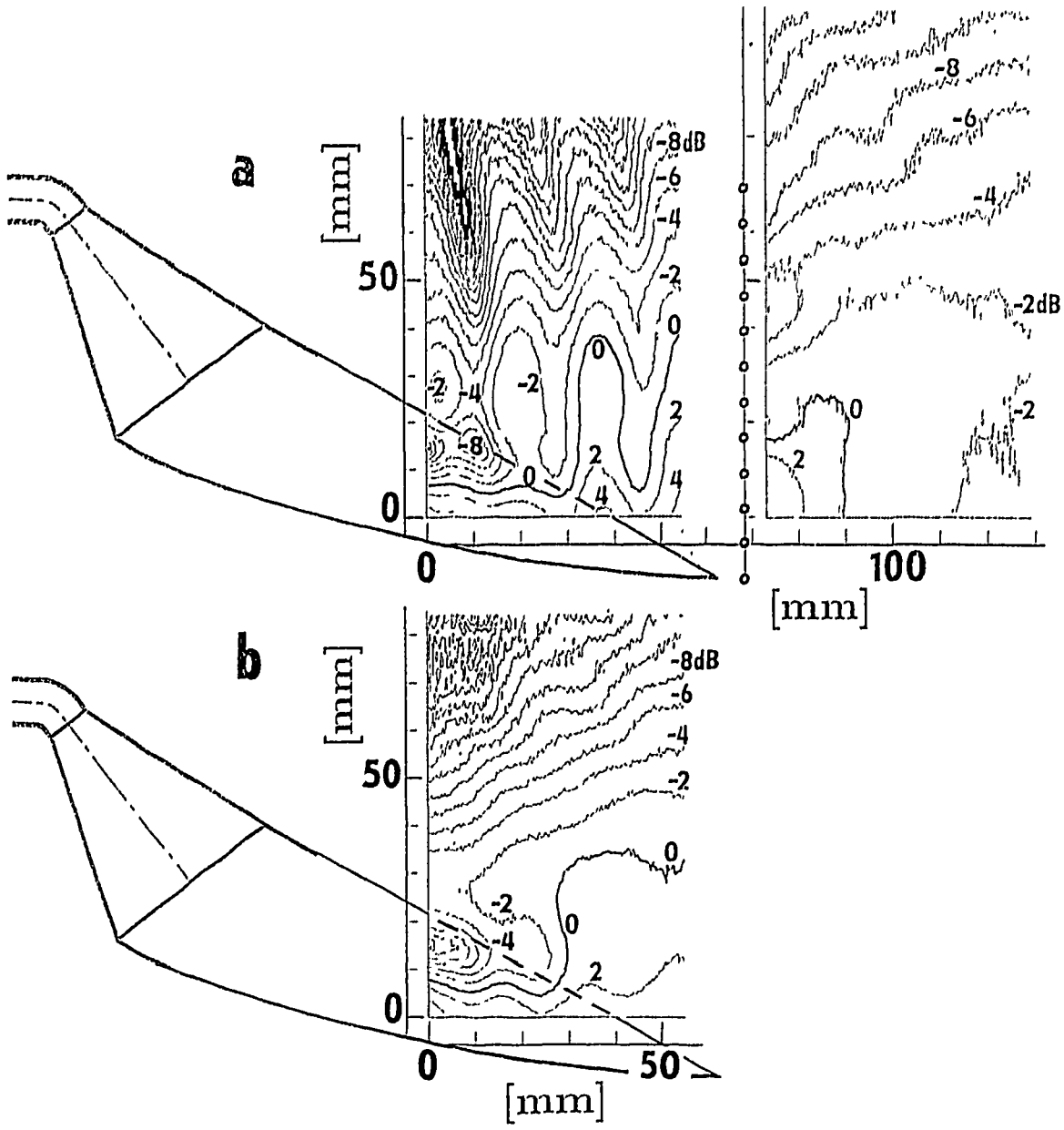

Figure 7: The radiation pattern in the same arrangement as given in Fig.6.

3 Project (design) of microwave antenna

The quasioptical launcher for lower hybrid waves calls for an oblique irradiation of diffracting rods by a plane wave. The paraboloid of revolution with a radiation source in focus can serve for this purpose if the plasma geometry is planar. Because the small radius of CASTOR tokamak is only 95mm the planar launcher would have bad coupling. We suggest that the coupler must have bended rods which follow the shapes of cylinders concentric with the plasma cylinder (we neglect toroidicity). Thus we need an oblique convergent cylindrical wave.

The problem can be easily solved in the frame of geometrical optics. We hope that this approach will be fruitful regardless that wavelength at 10 GH is only one forth of antenna dimensions and we work near the antenna. Some measurement of the shape of wavefronts supports this idea.

We choose the Cartesian coordinate with the z-axis parallel with the axis of plasma cylinder (the direction of the toroidal magnetic field of tokamak), the x-axis in the the equatorial plane (the centre of toroid lies in this plane) and the y-axis in the poloidal direction (the rods of quasioptical grill are parallel with this axis). The origin $F \equiv [0,0,0]$ coincides with the focus of our "paraboloidal" antenna or with "point-like" source of RF radiation.

The intersection of the equatorial plane ($y = 0$) with antenna is formed by the parabola. The angle of incidence φ of waves irradiating the rods is chosen equal to 25°. So that the parabola axis must contains the same angle with the x-axis. The parabola parameter (the distance between the focus and the apex) s is chosen equal to 30mm (from now all distances are in millimeters). The wall of box-limiter must be tangent to our antenna and also parallel to (x,y)-plane. From these conditions we obtain the coordinates of the contact point of the antenna and the wall $x_0 = 152, z_0 = 71$. This is placed at the mouth of the box-limiter (see Figs.1,2). The width of the mouth of the box-limiter in the z-direction at $x = x_0$ is 74mm thus $z_{\min} = -3$. The axis of the plasma cylinder is placed at $x_s = x_0 + 115$ (the distance between two rows of rods is equal 20mm and the small radius of tokamak is equal 95mm).

We determine the shape of antenna in the plane containing an angle θ with (x,z)-plane and going through the axis of plasma cylinder ($y = (x_s - x)\tan\theta$). In this plane the antenna must be formed by the intersection of this plane with paraboloid which has the focus at [0,0,0] and its axis is inclined by φ with respect to x-axis in (x,z)-plane and tilted by $90° - \theta$ from the y-axis. The length of the ray from the focus to the reflection point on antenna and further to the rows must not depend on θ. Thus we must increase the parameter s of the paraboloid after following rule $s = -121.1\cos\theta + 151.1$ (for the equatorial plane $\theta = 0$ and $s = 30$, for $\theta_{\max} = 20°$ we have $s = 41.3$). Our reflector consists of the infinitesimal strips corresponding to the individual θ for $\theta \in (-20°, 20°)$. The direction of ray was controlled and it was found that with astonishing preciseness coincides with that required by the cylindrical geometry.

The Fig. 8 shows the reflector in the orthografic projection (the waves are incident on the lower side of the surface). The front part (at $x \sim 160$) is cut circularly out to fit the shape of the plasma column. The side parts are defined by the rays with $\theta \pm 20°$. The reflector ends at plane $z = z_{\min} + (x_0 - x)\tan\varphi$) and thus the rays do not strike the opposite wall of the box-limiter at $z = z_{\min}$. The adequate horn must be added to the reflector to restrain rays from being incident out the surface of antenna.

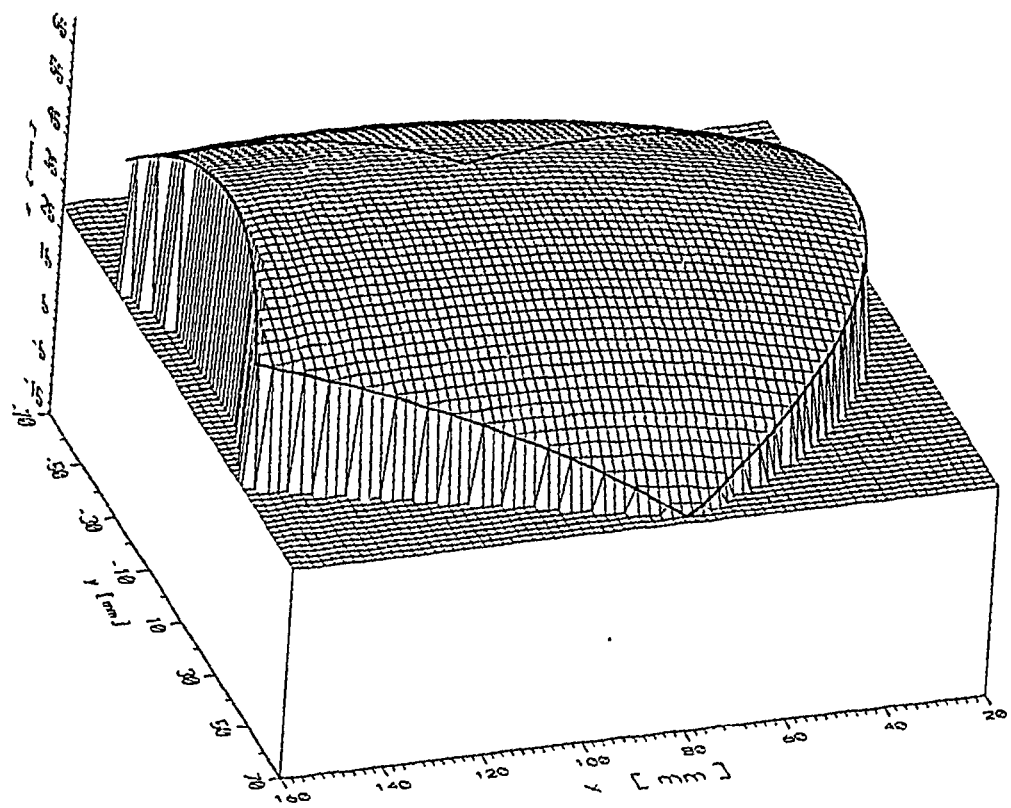

Figure 8: Design of the reflector in the orthographic projection (the waves are incident on the lower side of the surface.

4 Ray tracing

To facilitate finding the best position for direct measurement of LHW inside the plasma chamber, ray tracing calculations were performed for a chosen CASTOR regime ($n_e(0) = 7 \times 10^{18} m^{-3}, T_e(0) = 170eV, I_p = 6\ kA, B_T(0) = 1$ or $2T$, see Fig. 9). Within the flat top ($t = = 5$ ms to 10 ms), the average density falls down nearly twice; therefore, the calculations were made for $n_e(0) = 4.5 \times 10^{18} m^{-3}$ as well.

The ray tracing code used has been described in [6]. The equilibrium configuration of the magnetic fields (for prescribed initial radial profiles of the electron density and electron and ion temperatures) was obtained from the code ASTRA [7] (Automatic System of TRansport Analysis).

Fig. 10 offers, for the two marginal density profiles, the traces of rays launched at the equatorial, with the initial $N_{||} = 3.5$. No nonlinear effects are considered when reflections from the walls occur. The evolution of $N_{||}$ and N_{acc} along the ray path is also shown. In Fig. 11, only the first pass of rays launched at different poloidal positions (corresponding to the height of the grill) is given, in both poloidal and toroidal view, for $N_{||} = 3.5$ and -3.5. Fig. 12 illustrates the sensitivity of the ray paths to the change of the toroidal magnetic field, the electron density and the initial $N_{||}$.

From these figures, it seems that, technologically, the most simple way is to measure the LHW field after the first pass of the ray through the plasma via the auxiliary ports displaced roughly 45 degrees toroidally from the main port (indicated in the figures); the chance that the wave will be completely damped before reaching the wall is small in view of the low plasma temperature. However, the field maxima will move during the discharge due to the change in density.

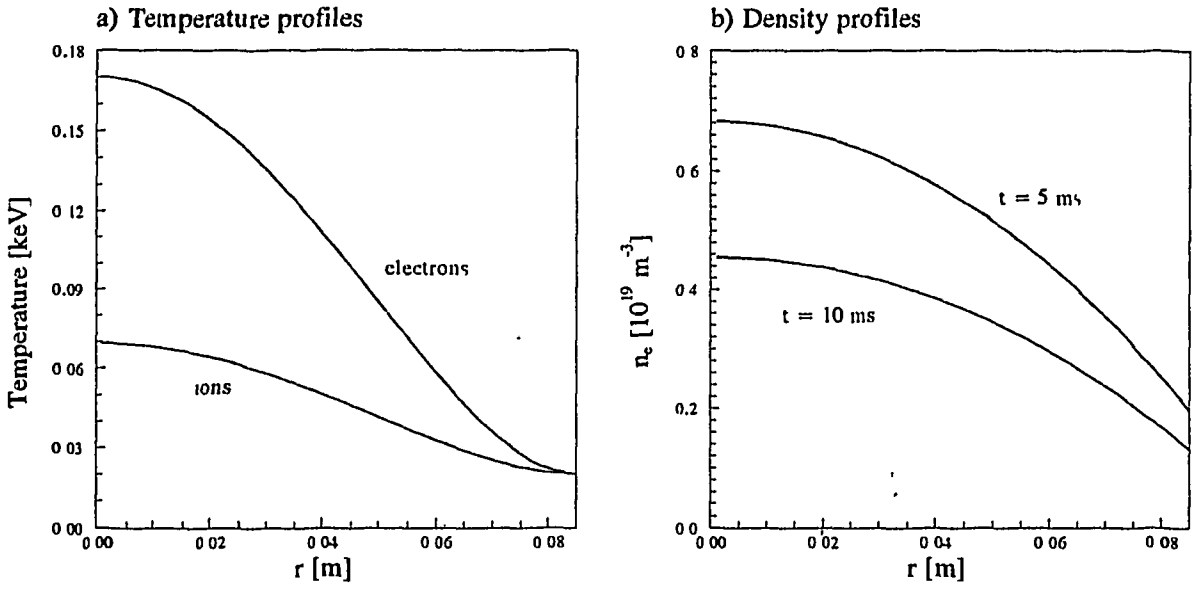

Figure 9: Radial profiles of plasma temperature and density.

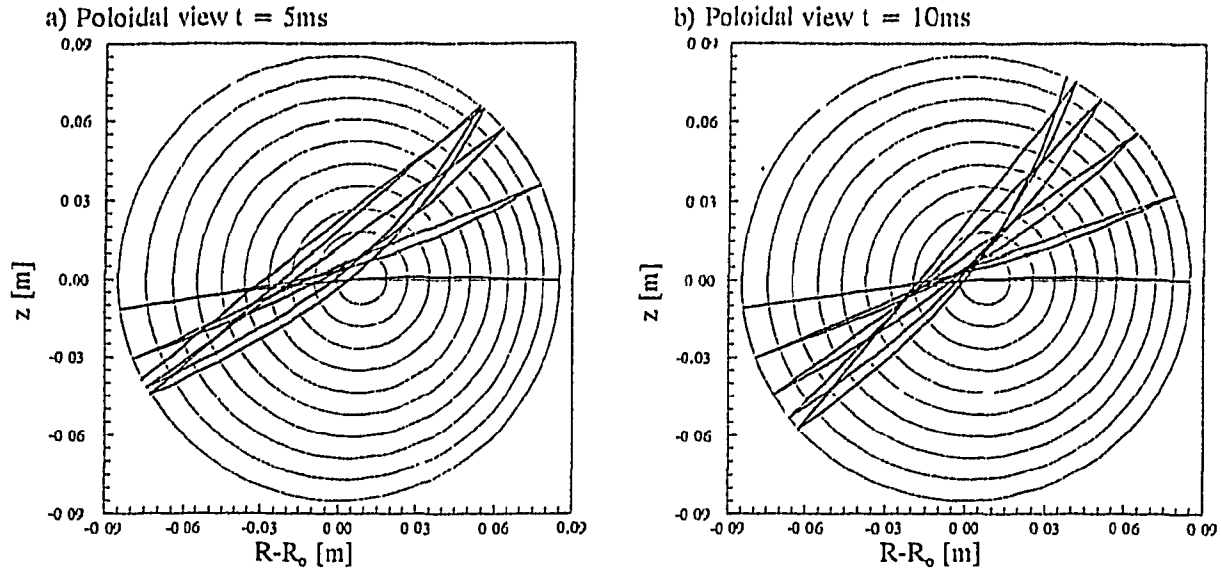

Figure 10: The path of a ray launched at the equatorial for the two density regimes, and the change of $N_{||}$ and N_{acc}.

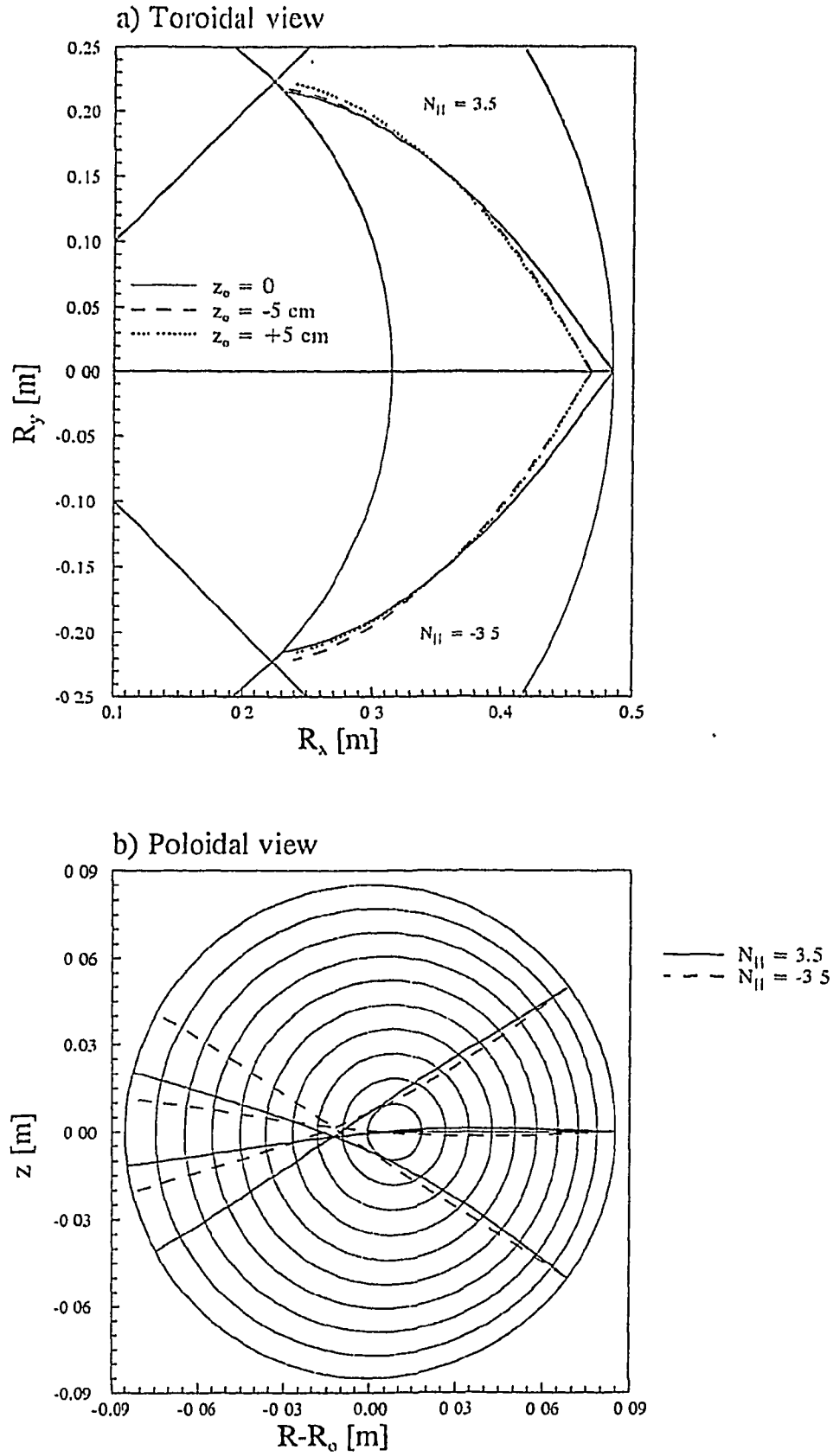

Figure 11: The paths of rays launched at various poloidal posisitons for $N_{\|} = +/-3.5$.

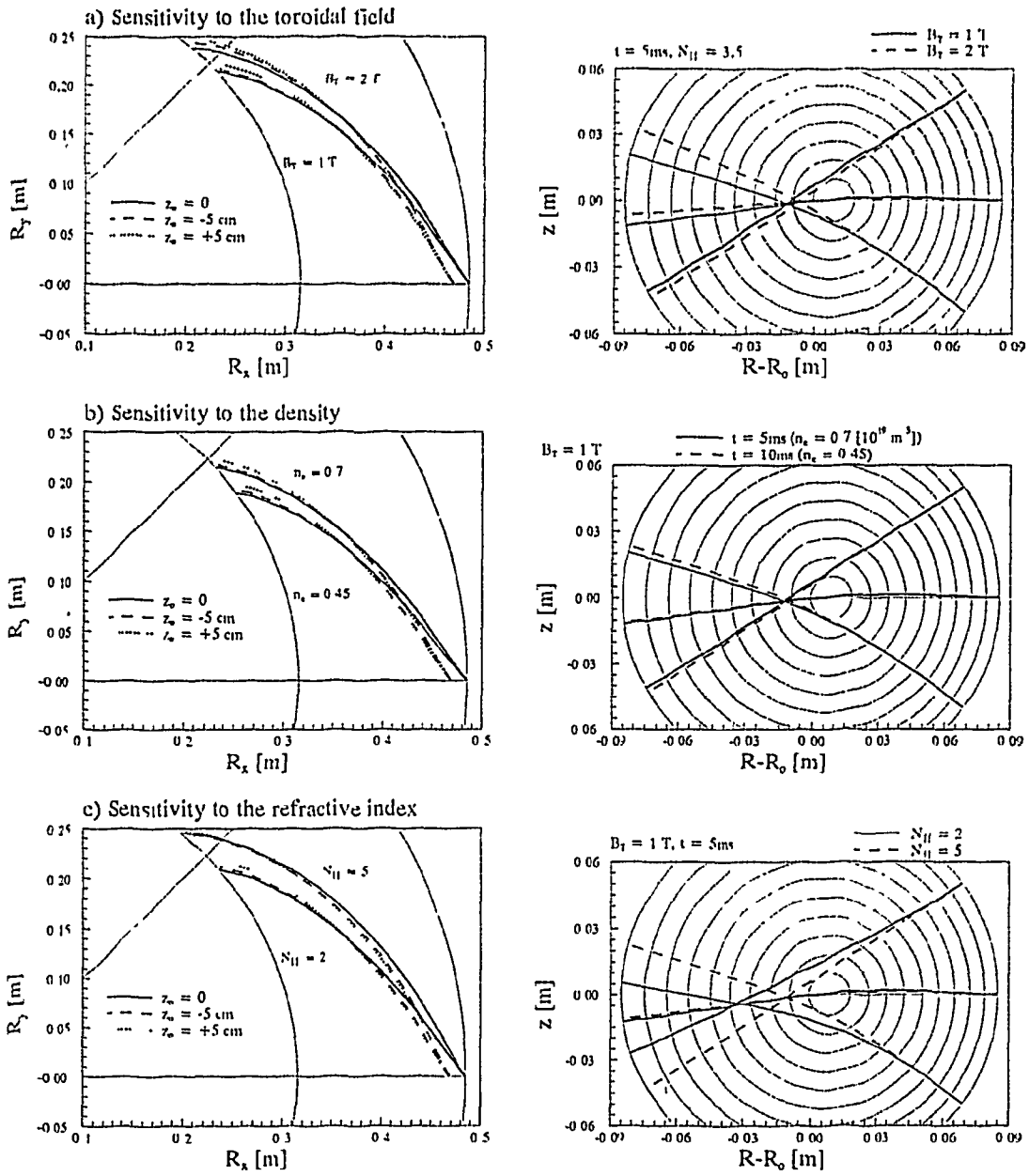

Figure 12: The change of the ray trajectories with the toroidal field, density and $N_{||}$.

5 Probing of the core plasma on the CASTOR tokamak

Quasioptical Grill (QOG) experiments, proposed to be done on the CASTOR tokamak, require detection of the slow electromagnetic wave by a double RF probe. The ray-tracing calculations show, however, that the slow wave will propagate under a quite large angle with respect to the toroidal magnetic field lines. One can expect, therefore, that the RF probe should be immersed rather deep into the plasma to reach the LH cone.

The described experiment demonstrates that, under specific discharge conditions, a material object, represented here by a single Langmuir probe, can penetrate into the core plasma without a significant perturbation of discharge.

Arrangement: A single Langmuir probe (tip diameter - 1mm, tip length - 3.5 mm, a stainless-steel sleeve of the diameter 4 mm) is movable on a shot to shot basis in the equatorial plane, see Fig.13. The probe is located $\sim 100^{o}$ toroidally away from the limiter section (in the anti-clockwise direction).

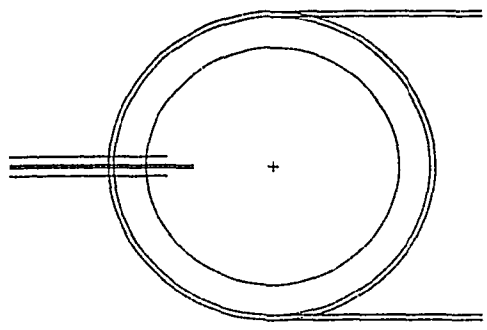

Figure 13: Arrangement of probe diagnostics.

The probe operates either in "Ion Saturation Current (ISC)" or "Floating Potential (FP)" modes.

Discharge: Experiments are performed at $B_t = 1\ T$. Regimes allowing the probe penetration into the core plasma are characterized by:
- short pulse operation (tokamak transformer is short-circuited in 10th ms),
- low plasma current ($I_p \sim 6\ kA$).

An example of discharge characteristics is shown in Fig.14.

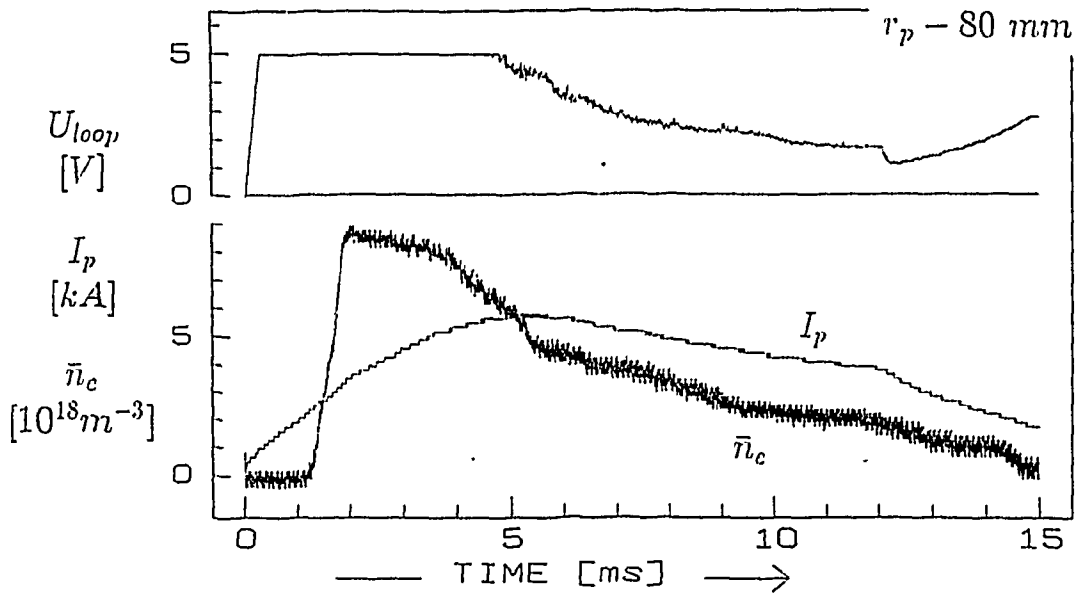

Figure 14: Evolution of low current shot.

Evolutions of loop voltage and plasma density are close to those in standard CASTOR 12 kA-shots ($U_{loop} \sim 2.5\ V, \bar{n}_e \sim 4 \cdot 10^{18} m^{-3}$). The central electron temperature is in the range of $T_e(0) = 150 - 170\ eV$ during the quasistationary phase of the discharge (derived from conductivity).

Probe signals: The evolutions of ion saturation current and floating potential are shown in Fig.15:
thick lines - the probe is at the plasma edge (limiter radius a = 85 mm),
thin lines - the innermost position of the probe.

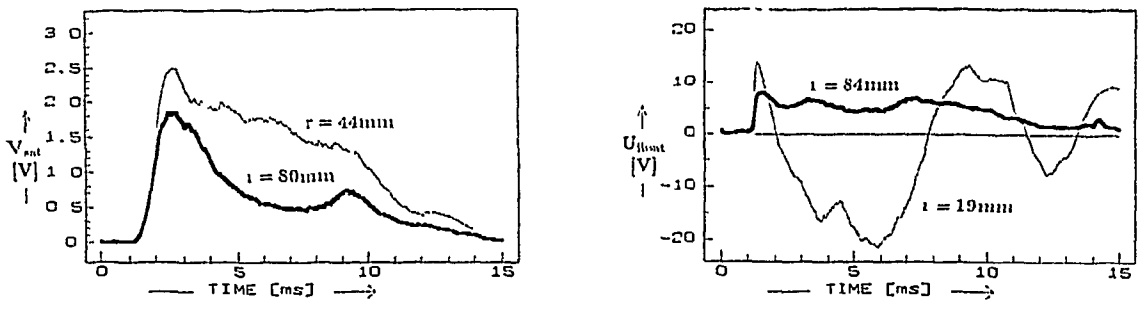

Figure 15: Evolution of probe signals.

The smooth form of evolutions (without any peaks) indicates a quite modest interaction of the probe tip with plasma under these particular discharge conditions.

Density profiles:
The local plasma density is estimated from the ion saturation current:

$$I_{sat} = 0.5 A n_i c_s \quad \Rightarrow \quad n_e \doteq 116 I_{sat}/\sqrt{T_e},$$

(A - the probe area, $c_s \sim \sqrt{T_e/M_i}$ - the ion sound velocity) assuming the following electron temperature profiles:

- initial phase - flat profile, $T_e = 7\ eV$ [8];
- quasistationary phase - parabolic profile

$$T(r) = [T(0) - T(a)][1 - (r/a)^2] + T(a);$$

T(0) = 170 eV, T(a) = 25 eV (according to our previous measurements [9]).

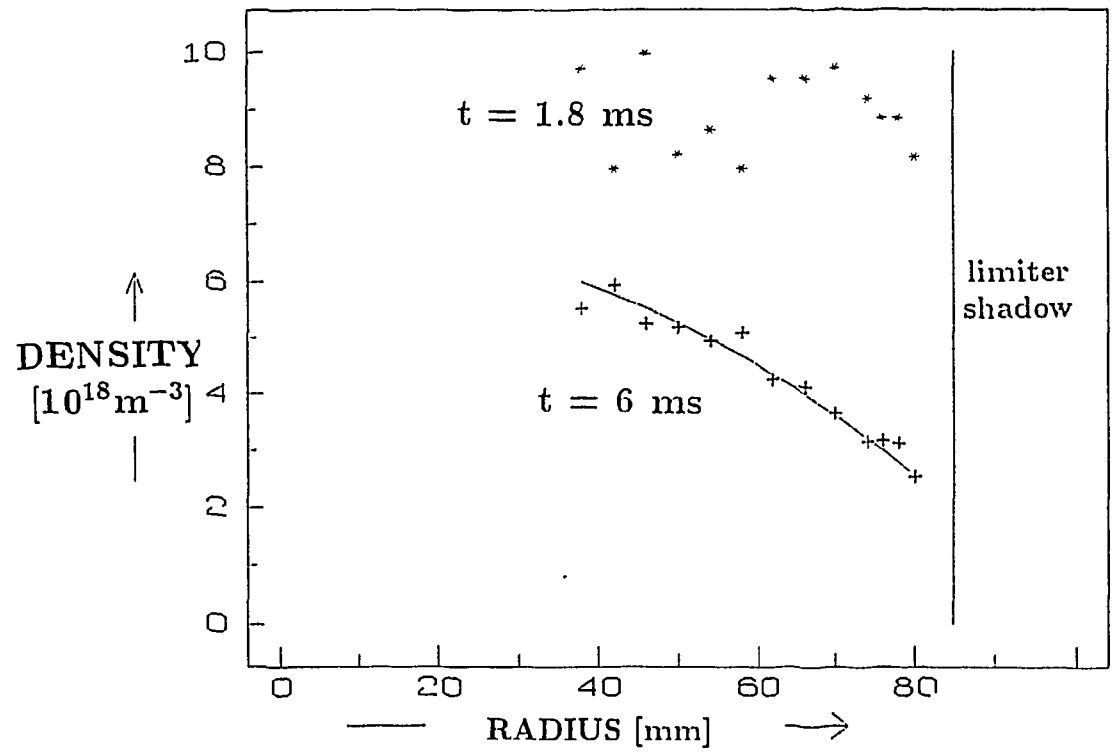

Figure 16: Density profile.

The initial density profile (t = 1.8 ms) is flat as expected. On the other hand, the profile during the quasistationary phase of the discharge (denoted by +) can be fitted to a parabola

$$n(0) = [n(0) - n(a)][1 - (r/a)^2] + n(a),$$

with $n(0) = 7 \cdot 10^{18} m^{-3}$ and $n(a) = 2 \cdot 10^{18} m^{-3}$, well corresponding to interferometer data.

Profile of floating potential: is shown in Fig.17:

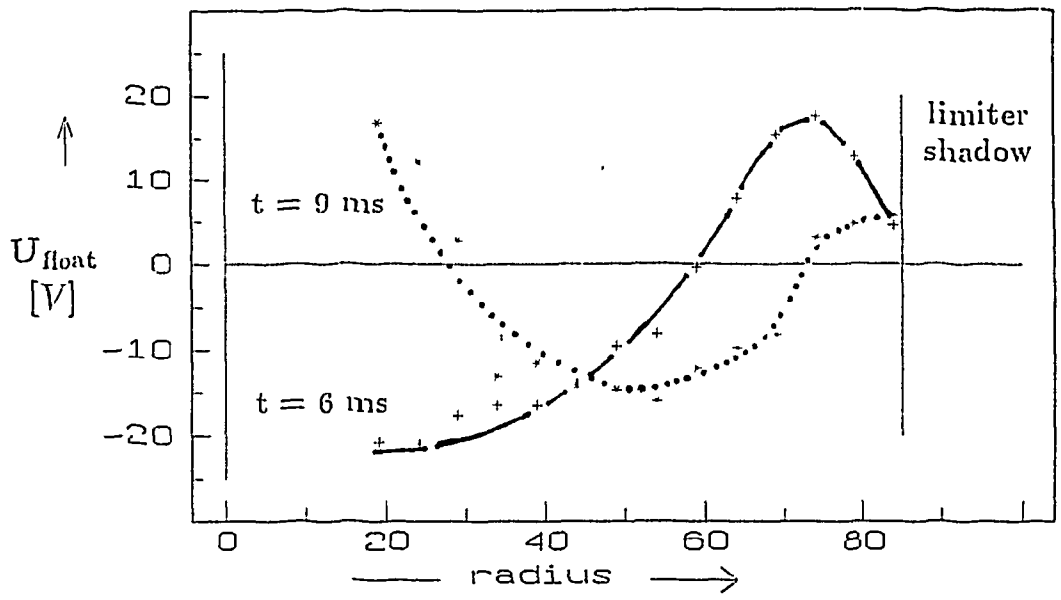

Figure 17: Profile of floating potential.

Finally, it can be concluded:

- A single Langmuir probe can be immersed into the plasma core ($r/a \leq 0.5$) without any significant disturbance of plasma. A short pulse length ($< 10\ ms$) and low plasma current ($< 6\ kA$) are required for the CASTOR case.

- The probe can penetrate in the plasma deeper in the "floating potential mode" than in the "ion saturation current mode":
  ISC-mode ... $r/a \sim 0.45$
  FP -mode ... $r/a \sim 0.22$.

- The double RF probes will operate just in FP-mode during the QOG tests. Therefore, a similar close approach to the plasma center as in the FP-mode can be expected.

- The next step will be a construction and similar tests of a double probe.

- We have obtained more or less realistic density and temperature profiles used further as input data for ray tracing calculations.

Acknowledgement
Work was supported by the grants GA CR No: 202/93/0711, G-IA 143103 and by IAEA Contract No: 6702/r1/rb.

References

[1] Pain M. et al.: "The Hyperguide: A New Concept of Lower Hybrid Launcher", Res. Rept. JET-P(92)94

[2] Petelin M.I., Suvorov E.V., Sov. J. Tech. Phys. (letters) 15 (1989), 882

[3] Klíma R.: "Preliminary considerations on the diffraction (quasi-optical) grill in CASTOR tokamak", Res. Rep. IPPCZ-335, Prague 1993

[4] Frezza F., Gerosa G., Gori F., Santarsiero M., Santini F. and Schettini G.: Meeting on Advanced Launchers, Frascati, Oct. 1993

[5] Goldberg A.V., Kovalev N.F., Petelin M.I., Suvorov A.V. and Filchenkov S.E.: Private communication, August 1993

[6] Pavlo P., Krlín L., Tlučhoř Z.: Nucl. Fusion 31 (1991), 711.

[7] Pereverzev, G. V., Yushmanov, P. N., Dnestrovskiy, A. Yu. et al., Rep. IPP Garching No. 5/42 (1991).

[8] A. Raicu et al: Czech. J. Phys., B37, 1987, p.850

[9] J. Stöckel et al: EPS -Lisabon 1993, Vol.2., p.691